CHARACTERIZATION OF THE IMAGING PERFORMANCE OF A PORTABLE, CODED-APERTURE, GAMMA-RAY IMAGER FOR USE IN ENRICHMENT PLANTS

Benjamin T. Dabbs[b], Jason P. Hayward[a,b], Klaus-Peter Ziock[a],
Chris B. Boehnen[a], James S. Bogard[a], Ana C. Raffo-Caiado[a]
[a]Oak Ridge National Laboratory, Oak Ridge, TN 37831
[b]The University of Tennessee, Knoxville, TN 37996

ABSTRACT
The imaging performance of a mechanically cooled, portable, coded-aperture, gamma-ray imager designed for international safeguards inspections at uranium enrichment plants has been characterized. The imaging performance of the instrument was quantified by calculating the signal-to-noise ratio as a function of the source distance, position, enrichment, and acquisition time. Based on the expected international safeguards application, importance has been given to the use of uranium standards enriched to less than five percent at source-detector distances greater than two and one-half meters. The implications of the results for the utility of the instrument for safeguards work are discussed.

INTRODUCTION
The ability to combine a three-dimensional (3D) laser scanner with a HPGe-based, coded-aperture, gamma-ray imager [1] was demonstrated during a measurement campaign conducted in a chemical makeup area at Oak Ridge National Laboratory (ORNL). During this campaign, the coded-aperture imager was capable of detecting a 4.46% enriched source of 7.54 g ^{235}U at a distance of 1.8 meters with a 400 second total acquisition time [2]. Such measurements using this combined system allow international safeguards inspectors to verify that the process system design, as well as the location of nuclear materials, are consistent with the operator's declaration. In addition, this combined system has the ability to detect undeclared nuclear materials.

The end application of the project is to perform measurements in operating uranium enrichment facilities. To prepare for such field tests, the performance of the coded-aperture imager is currently being characterized in a laboratory setting with respect to source enrichment, source-detector distance, source position within the field-of-view (FOV), and acquisition time. To be useful for international safeguards inspections, it is desirable that the combined system be able to image low enriched uranium (LEU) at distances greater than two and one-half meters.

The work is being conducted in the framework of technical cooperation agreements between the U.S. Department of Energy (DOE) and the European Atomic Energy Commission (EURATOM) and between DOE and the Brazilian-Argentine Agency for Accounting and Control of Nuclear Materials (ABACC). The complete collaboration includes the following DOE national laboratories: ORNL, Lawrence Berkeley National Laboratory (LBNL), and Lawrence Livermore National Laboratory (LLNL). The effort also relies on the technical support and expertise from two regional safeguards organizations: EURATOM's Joint Research Centre at Ispra, Italy (JRC-Ispra) and ABACC.

CHARACTERIZATION OF DETECTOR

The performance of the coded-aperture imager (see Figure 1) has been characterized with respect to uranium enrichment, source-detector distance, source position within the FOV, and acquisition time.

Uranium standards enriched to 1.94% and 4.46% ^{235}U were used for these measurements. The standards consisted of 200 g U_3O_8 powder with an area density of 5.2 g/cm^2 contained in an aluminum can of right cylindrical geometry with an active diameter of 70 mm. The bottom of the source cylinders was oriented parallel to the surface of the imager. Due to self-attenuation, the amount of ^{235}U contributing to the signal is much less than that contained within the standard. A simple numerical integration was performed and found that the equivalent mass of ^{235}U being measured from the 1.94% and 4.46% enriched 200 g standards is approximately 0.40 g and 0.95 g, respectively.

Data were acquired for these sources located in the center of the FOV (see Figure 2) at 3, 4, and 5 meters with a constant focal length (spacing between the mask and detector) of 7.5 cm. This focal length selection allows for the widest FOV and largest pixel size for a given distance to the object being imaged to ensure the measurement of point-like sources. The respective pixel sizes for this focal length and source distances of 3, 4, and 5 meters are 5.7 cm, 7.5 cm, and 9.4 cm.

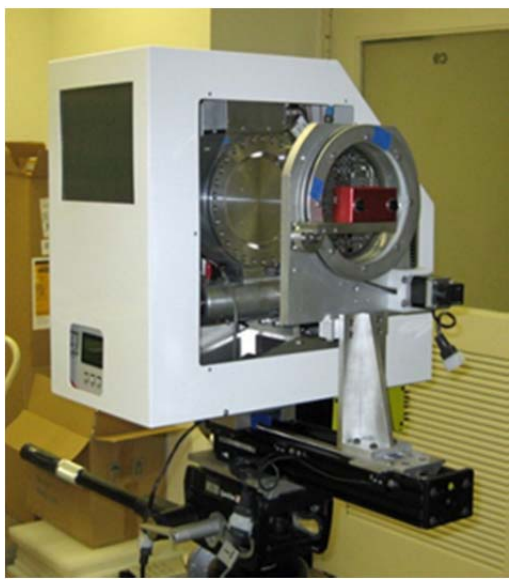

Figure 1. Photograph of portable, coded-aperture, gamma-ray imager including cover, touch screen computer, and stereo imager. The imager is mounted on a tripod.

In this study, the ability to image was quantified by the ability to detect, which was in turn quantified by the signal-to-noise ratio (SNR). The SNR was calculated by dividing the number of counts in the image pixel in which the source was located by the root mean square (RMS) deviation (measure of fluctuation around the mean) of the counts in the image pixels in which the source was

absent. This is a first order approximation derived from the imaging properties of coded apertures that means each of the pixels in the image has approximately the same variance. This is a direct result of the cross-correlation function used with the measured shadow pattern and the known mask function:

$$I_{i,j} = \sum_{m,n} M_{i+m,j+n} D_{m,n} \quad (1)$$

Here $I_{i,j}$ is the number of counts in pixel (i,j) of the image, and $M_{m,n}$ and $D_{m,n}$ are the mask function and detector counts, respectively. The mask function is either plus or minus one depending on whether the mask pixel is either open or closed, respectively. As implied by Equation 1, all counts in the detector contribute to every image location.

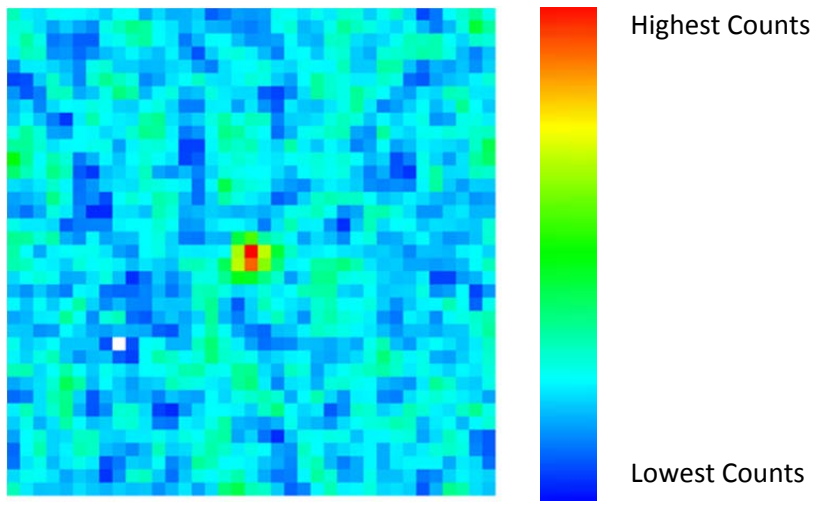

Figure 2. Detector image showing 1.94% enriched source located in the center of the FOV after 48 hours of total acquisition time. The regions of highest counts are red, while the regions of lowest counts are dark blue.

The data were acquired in list-mode to enable replaying with different parameters. In this case, each data set was subdivided into multiple time intervals at each distance to generate the plots shown in Figures 3 and 4. The results are based on an energy window (±3 keV) limiting the data to only the 186-keV peak of ^{235}U. The detector data were then exported and analyzed to calculate the SNR as described above. The results show the expected linear relationship between the square root of the acquisition time and SNR that arises from the fact that the uncertainty in the signal, S, given by

$$SNR = \frac{S}{\delta S} \propto \frac{T}{\sqrt{T}} \propto \sqrt{T} \propto \sqrt{t} \quad (2)$$

is equal to the square root of the total number of counts, T, in the selected energy window. In turn, T is proportional to the acquisition time, t. By fitting a linear trendline to the data, an appropriate acquisition time can be determined to achieve a desired SNR. For this analysis, a SNR value of five was chosen as the minimum needed to signify detection. This SNR corresponds to a false alarm probability of approximately one in 2,000,000. Each image contains ~350 resolution elements, however, so that the true false alarm rate per image is approximately one in 5,500.

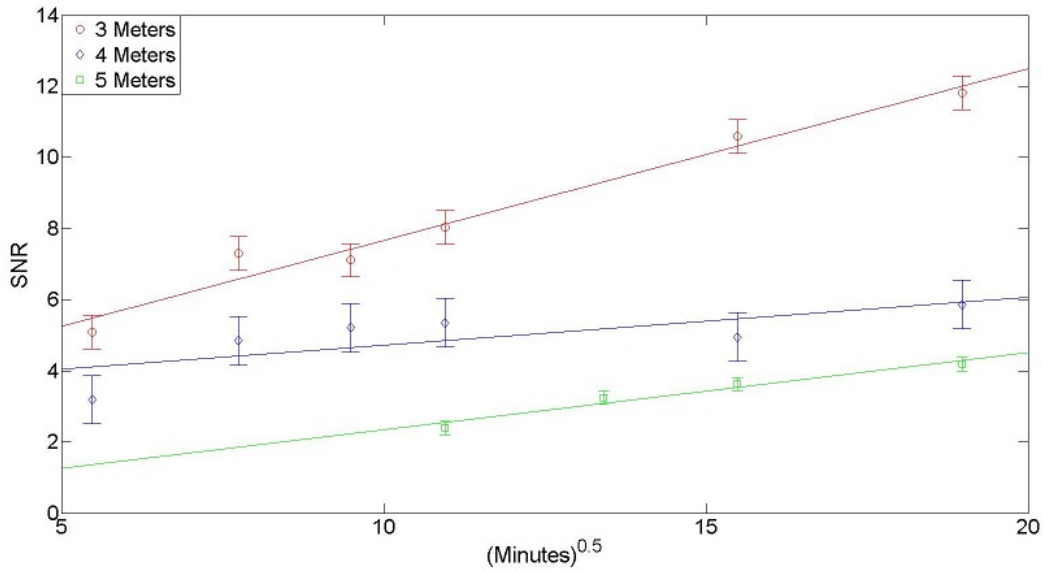

Figure 3. SNR vs. square root of the acquisition time for a 4.46% enriched uranium standard at 3, 4, and 5 meters.

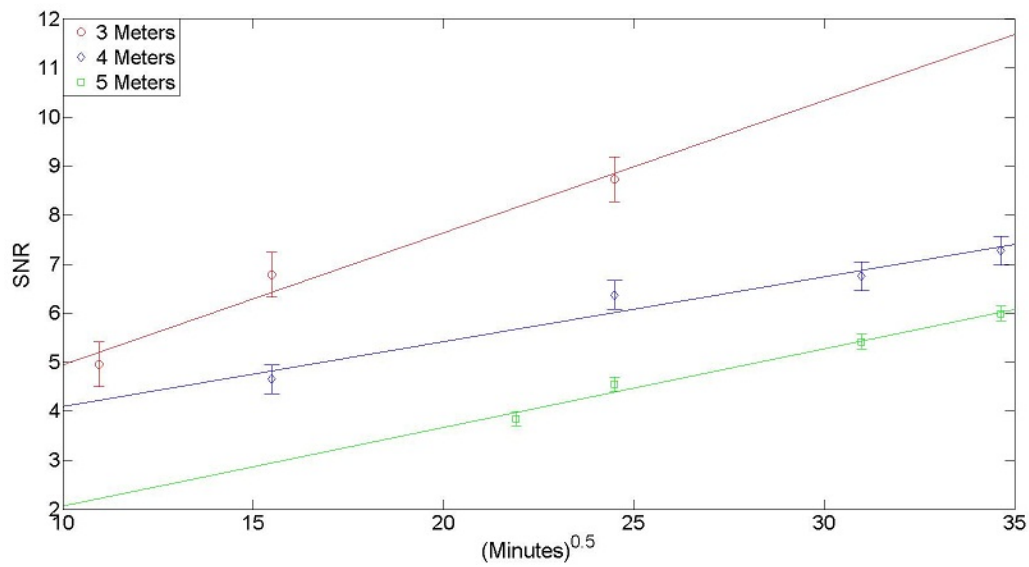

Figure 4. SNR vs. square root of the acquisition time for a 1.94% enriched uranium standard at 3, 4, and 5 meters.

Once the necessary acquisition time to achieve this value of SNR was determined for each distance, a plot was generated of distance versus time (see Figure 5). Due to self-shielding effects, the time for detection of a particular mass of 1.94% or 4.46% enriched uranium is expected to depend greatly on the geometrical configuration of the source. It is also important to note that the SNR values will depend on both the radiation from the source as well as the background radiation within the imaging environment. The effect of background upon SNR in an enrichment plant environment will be a subject of study for the upcoming field trial.

It is expected that the time to achieve detection at a specific distance should decrease linearly as the equivalent mass of ^{235}U (m_{235}) increases:

$$SNR = \frac{S}{\delta S} \propto \sqrt{T} \propto \sqrt{m_{235}} \quad (3)$$

Combining Equation 2 and Equation 3 illustrates this relationship by showing that the equivalent mass of ^{235}U is proportional to the acquisition time. Additional data is needed, however, to verify this relationship.

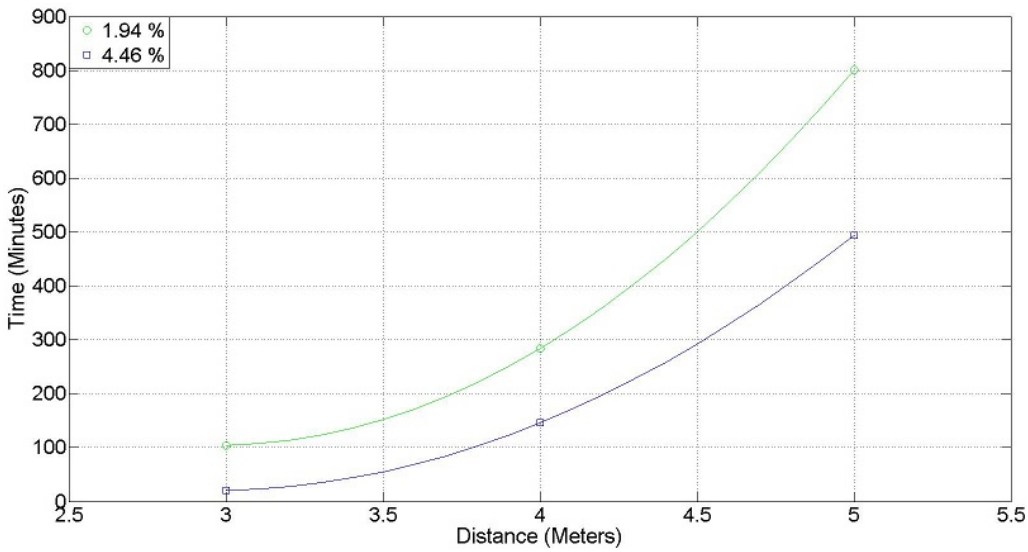

Figure 5. Distance vs. time to achieve a SNR value of five for a 1.94% and 4.46% uranium standard.

ALTERNATIVE SNR METHOD

For comparison, an alternative method of calculating SNR was analyzed. As mentioned, the method used above is based on a first-order approximation assuming the variance in each image pixel is nearly equal. The alternative method does not rely on this approximation, as it takes into account the fact that data in adjacent image pixels could be correlated. The data sets were subdivided into shorter time intervals and a 2D Gaussian function of the form

$$N = A_0 + A_1 e^{-(A_2-x)^2/{A_3}^2} e^{-(A_4-y)^2/{A_3}^2} \quad (4)$$

was fit to the source region of each segment using a chi-square minimization procedure [3]. Here, A_0 is the baseline, A_1 is the amplitude, A_2 is the x-location, A_3 is the width, and A_4 is the y-location. The SNR was then calculated from

$$SNR = \frac{S}{\delta S} = \frac{S_{avg}}{\sqrt{{\sigma^2}_{amp} + {\sigma^2}_{baseline}}} \quad (5)$$

by dividing the average peak height (amplitude - baseline), S_{avg}, by the square root of the sum of the squares of the uncertainty in the amplitude and baseline. An assumption here is that a Gaussian

function can be fit well to the measured data. The results, along with the original results, for the 1.94% enriched standard at 3 and 4 meters are shown in Figure 6 and Figure 7, respectively.

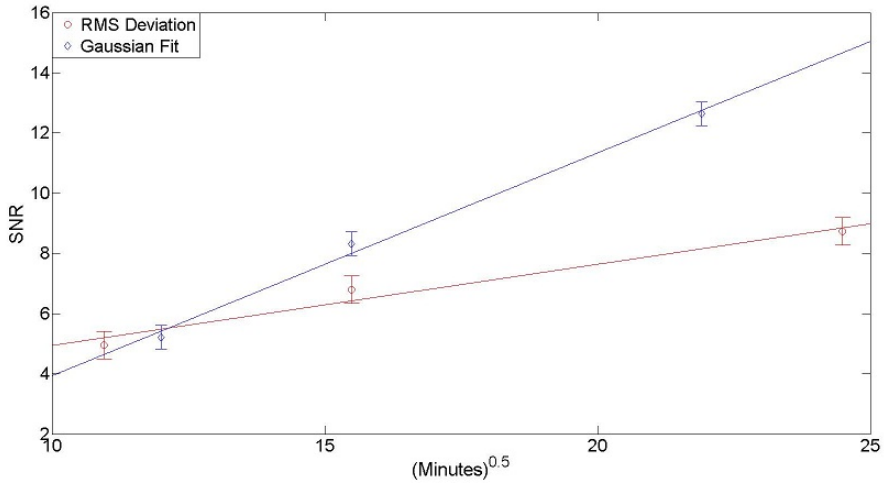

Figure 6. Plot comparing results from the different methods of calculating SNR for 1.94% enriched standard at 3 meters.

As seen, the two methods provide very different results. At 3 meters, the RMS deviation method achieved a SNR value of 5 after ~105 minutes, while the alternative (Gaussian fit) method required ~130 minutes. At 4 meters, however, the RMS deviation method achieved detection in ~280 minutes, while the alternative method required ~470 minutes for the detection. As the source-detector distance increases, the Gaussian fit parameters become more inconsistent between segments due to the decreasing amount of data to be fit. The signal decreases from 3 to 4 meters, as expected, but because of the inconsistent fit parameters, the uncertainty increases. At distances greater than 4 meters, the data is not capable of being fit to a Gaussian unless much longer acquisition times are used. For these reasons, the original method remains the best for this analysis.

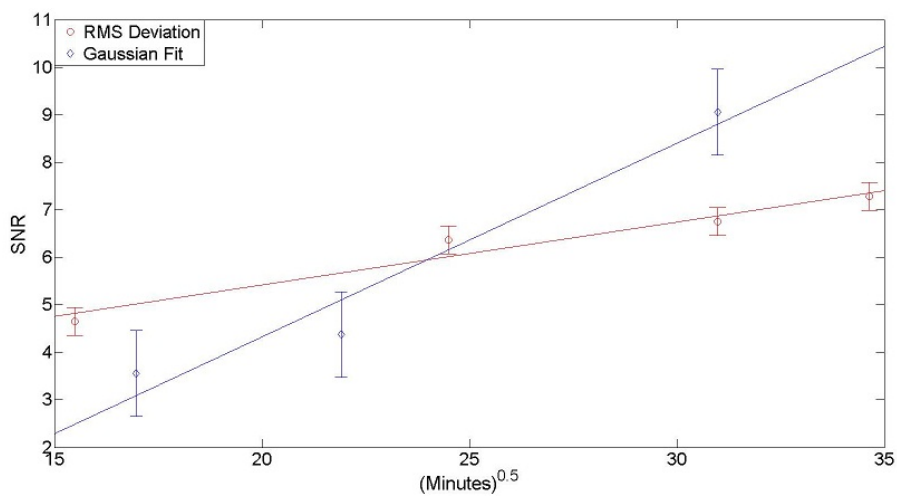

Figure 7. Plot comparing results from the different methods of calculating SNR for 1.94% enriched standard at 4 meters.

ANALYSIS OF SOURCE LOCATION

Data are being collected and analyzed to further study the performance of the detector with respect to additional parameters. For instance, the efficiency for detection of a source will vary as a function of location in the FOV. This has been measured using a 97% enriched uranium source. The data were collected at a distance of 3 m with a 7.5 cm focal length within the lower right quadrant of the FOV. With the assumption that this response is symmetric to the response in the remaining three quadrants, the data was replicated across the FOV to produce the plot shown in Figure 8 [4].

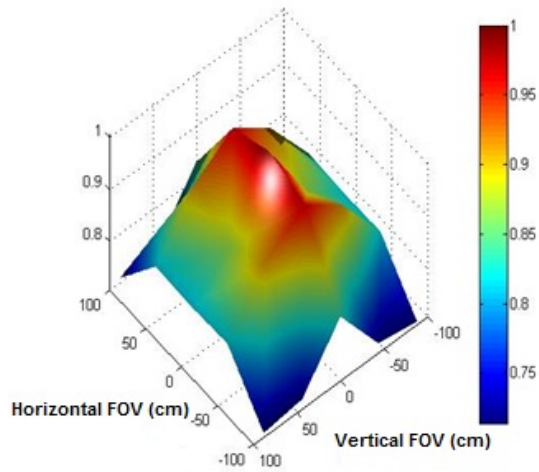

Figure 8. Normalized data showing the efficiency for detection as a function of source location.

The falloff in sensitivity at the edges of the FOV is larger than expected as compared to simulations of these measurements. The simulations used a mask of appropriate thickness and relied on the following assumptions: (1) the mask is infinitely opaque so that any photon that strikes a non-open location will be lost (an over assumption that should make the simulated falloff more severe); and (2) the detector has no thickness so that each photon is recorded in the correct pixel. These simulations predicted a maximum falloff at the corners of the FOV of approximately 10-15%, while the measurements gave a falloff of approximately 25-30% at the same locations. There are a few factors that contribute to this: first, there is a falloff in projected detector area as the source is moved off axis, which varies as the cosine of the angle to the source and has been corrected for in the figure. Of the remaining falloff, approximately half can be attributed to self-collimation effects due to the finite thickness of the mask. The causes of the additional falloff are still under investigation.

USE OF DIFFERENT URANIUM SPECTRAL LINES

As previously mentioned, for a given measurement, the system performance will depend on the level of background radiation compared to the flux from the source. This can be influenced by selecting different regions of interest in the spectral data. The relatively unshielded material used in these studies shows not only the 186-keV line but also flux at 144 keV and atomic fluorescence lines around 100 keV. The relative proportions of these lines will depend on the enrichment and geometry of the material as seen in Figure 9 (the amount of material, integration times, and source

location were not controlled to allow comparison of absolute numbers between the samples) [4]. The results in Table 1 show how the selection of different energy windows influences the SNR of the 1.94 % enriched standard at 4 meters for a total acquisition time of 48 hours. Of course, the emissions from the process equipment will be preferentially shielded at lower energies, reducing the contributions from the lower energy lines. Although collecting data using spectral lines other than the 186-keV line can reduce the dwell time required to make detection, optimization for a given situation will need to be performed.

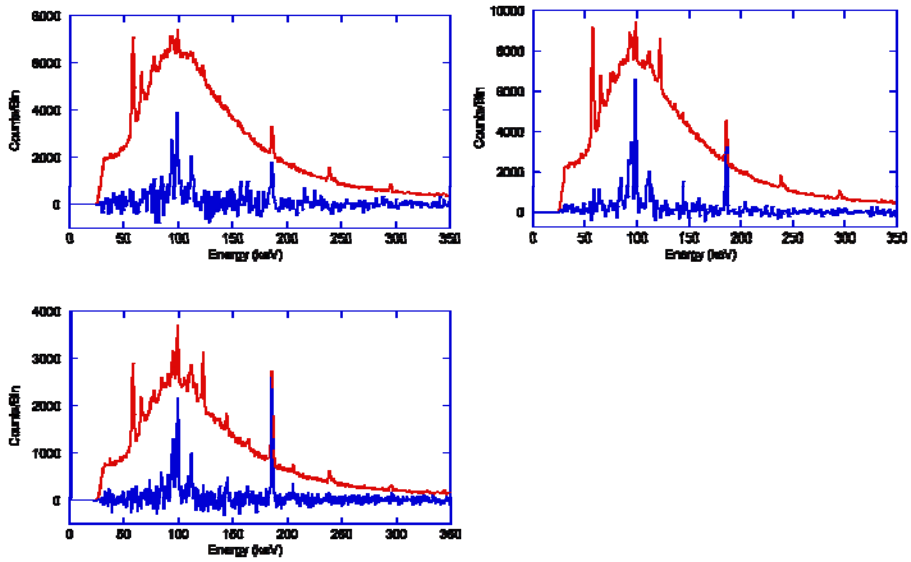

Figure 9. The red spectra are from the detector as a whole. The blue spectra are from the localized source region of the image. Note the difference in relative line intensities for the different samples: 1.94% (top left), 4.46% (top right), and 93.17% (bottom left). The localized (blue) spectra are inherently background subtracted due to the imaging process of Equation 1.

Table 1. SNR versus spectral regions.

	All Energies	181–189 keV	90–101 keV 181–189 keV	90–101 keV 141–146 keV 181–189 keV	90–189 keV
SNR	11.2	8.2	14.7	13.8	12.6

NEXT STEPS

Following characterization of the coded-aperture imaging system in a laboratory setting, it is important to test the instruments in a realistic field trial. Although the final goal is to perform measurements and to demonstrate the usefulness of the instruments in facilities monitored by EURATOM and ABACC, an initial field test will be performed at the Paducah Gaseous Diffusion Plant (PGDP). In addition to the coded-aperture imager and the 3D Laser Scanner, another gamma-ray imaging instrument (Compton imager) will be used. These two imaging techniques are complimentary to each other in the fact that this coded-aperture imager has been optimized for energies around 186 keV and below a few hundred keV, while Compton imagers are best suited for energies above 300 keV.

Other goals and potential benefits for these measurements include: (1) determining dwell times required by the different gamma-ray imagers in operating enrichment facilities; (2) providing facility personnel a non-intrusive method for determining the volumetric and isotopic distribution of holdup deposits in cascade piping as well as other process equipment; and (3) providing accurate knowledge of material inventories which can lead to additional benefits such as reduced costs and simplified procedures. An additional objective for these measurements is to demonstrate that the different data sets can be combined in real-time. To ensure this is feasible, an additional computer will be set up to perform this task onsite throughout the measurement campaign.

Information gathered from discussions with the United States Enrichment Corporation (USEC) and during a preliminary site visit has identified possible locations for the measurements. The locations were chosen as a result of the material being in a condensed state which provides a greater flux of gamma radiation per unit volume. In interest of showing the strength of the Compton imager, some locations have been chosen with solid deposits in which the 1001-keV line from ^{234m}Pa (decay product of ^{238}U) is evident.

CONCLUSIONS

The response of a portable, HPGe-based, coded-aperture, gamma-ray imager has been characterized for the detection of low enriched uranium standards with gram quantities of ^{235}U at standoff distances greater than two and one-half meters. For the 1.94% enriched standard, a SNR value of 5 was achieved at 3, 4, and 5 meters with total acquisition times of approximately 105, 280, and 800 minutes, respectively, while the 4.46% enriched standard achieved this in approximately 20, 145, and 495 minutes, respectively. Due to self-attenuation effects, this analysis reflects ^{235}U masses of approximately 0.40 g for the 1.94% enriched standard and 0.95 g for the 4.46% enriched standard. If equivalent masses of ^{235}U and distances measured are indicative of those present in enrichment plants, measured times to detection show that tens of minutes to hours are required for a point-like source. Future work will include repeating the above analysis with standards of different enrichments and performing measurements with the source in different locations within the FOV to better understand the response of the detector as a function of position.

REFERENCES

1. K-P. Ziock et al., "Mechanically-Cooled, Highly-Portable, HPGe-Based, Coded-Aperture Gamma-Ray Imager," *Proceedings of the 51st INMM Annual Meeting*, July 11–15, 2010, Baltimore, Maryland, 2010.

2. A. C. Raffo-Caiado et al., "Combining Measurements with Three-Dimensional Laser Scanning System and Coded Aperture Gamma-Ray Imaging System for International Safeguards Applications," *2010 IAEA Symposium on International Safeguards*, November 1–5, 2010, Vienna, Austria, 2010.

3. W.H. Press, S.A. Teukolsky, W.T. Vetterling, B.P. Flannery, Numerical Recipes in C (Cambridge University Press, 1995) pp 683-687.

4. Benjamin T. Dabbs et al., "Characterization of the imaging performance of a portable, coded-aperture, gamma-ray imager for use in enrichment plants," *33rd ESARDA Annual Meeting*, May 16-20, 2011, Budapest, Hungary, 2011.